ELECTROLYTIC GENERATION OF TRAPPED NANOBUBBLES VIA NUCLEATION CORE WITH PICOLITER PRECISION

Eugene Yoon and Ellis Meng
University of Southern California, Los Angeles, California, USA

ABSTRACT

A design configuration and methodology for control of electrolytic generation of gas bubbles within microfluidic devices is presented that achieves decreased power consumption and improved volume precision. Electrolytic generation of single trapped nanoliter-microbubbles within microchannels at picoliter precision ($\sigma_{\bar{x}}$ down to 1.1 pL) was achieved by employing a large surface area counter electrode (CE). We also attained reduced energy consumption (up to 44%). Micro and macro CEs with areas spanning five orders of magnitude were evaluated while holding the micro working electrode (WE) area constant. To the best of our knowledge, this is the first investigation into the relationship between CE size and nanobubble volume repeatability with implications on electrochemical bubble-based microfluidic devices.

KEYWORDS

Nanobubble, microbubble, microfluidic, electrolysis, precision, Parylene C, electrochemistry, Faradaic reaction

INTRODUCTION

Electrolytic bubbles can be generated on-demand and have several advantages leading to their application in MEMS pumps [1], valves [2], actuators [3], contrast agents [4], and sensors [5]. However, to date, these devices used only microscale electrodes (<1 mm^2) for the WE and CE.

While microelectrodes preserve a small device footprint, this design choice results in several consequences: increased power consumption and decreased repeatability of generated gas volume. Since the electrode-to-electrolyte voltage (not electrode-to-electrode) drives Faradaic gas evolution [6], one strategy to improve efficiency is to confine the voltage drop to the WE-electrolyte interface (Fig. 1).

This strategy can be implemented by using a macroscale CE with large surface area in lieu of a microelectrode to increase the double layer capacitance (C_{dl}) of that electrochemical interface. Due to electroneutrality, the same amount of charge is applied at the WE and CE whenever a current/voltage is applied between them. At the CE-electrolyte interface, most of the charge is spent on charging C_{dl} so Faradaic reactions do not occur appreciably. In contrast, the WE-electrolyte interface C_{dl} is quickly charged beyond capacity and most of the charge is therefore spent on Faradaic gas evolution. This ideal configuration effectively and efficiently localizes electrode polarization to the WE with only a simple modification to the device design. If both WE and CE are similarly sized microelectrodes, energy is wasted in polarizing both (non-ideal case).

To achieve precise nanobubble volume control, we investigated the effect of CE surface area on nanobubble generation at a microscale WE within a microchannel. Surface inhomogeneities on electrode surfaces are known to affect the repeatability of electrochemical reactions and the additional surface area of a larger CE was hypothesized to minimize such effects because the relative ratio of contaminated vs. nominal surface area is more favorable than that of smaller CEs.

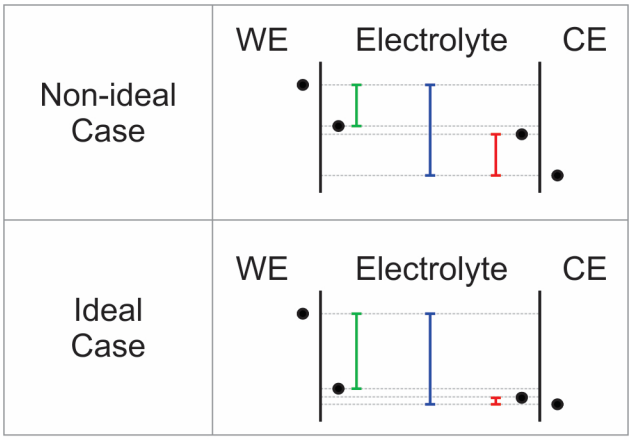

Figure 1: Electrochemical potential diagrams showing voltage drop magnitude at the WE-electrolyte (green) and CE-electrolyte (red) interface. Ideally, the drop should be localized at the WE-electrolyte interface. The total applied voltage is indicated in blue.

For this work, generation of single nanobubbles within a microchannel was investigated (Fig. 2). The nanobubble was generated within a nucleation core containing the WE and directed into the adjacent microchannel. This format is necessary to position the generated bubble away from any exposed, catalytic Pt microelectrodes and prevent gas recombination. The larger microchannel also facilitated optical analysis.

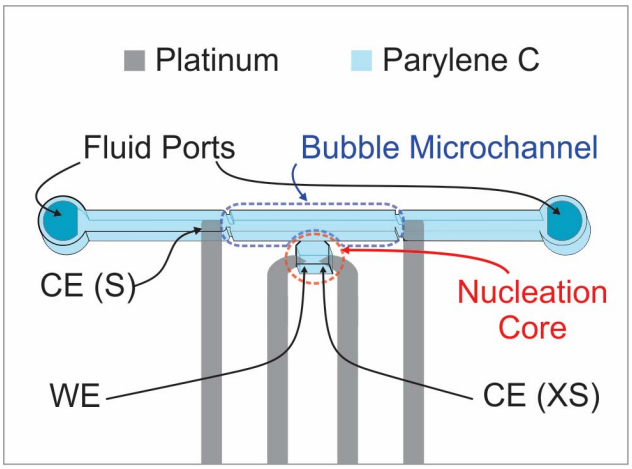

Figure 2: Schematic diagram showing main device components. The working electrode (WE) is used with different counter electrodes (CE) within and external to the device to generate the nanobubble.

MATERIALS AND METHODS

Parylene surface micromachining was used to fabricate microchannel structures containing exposed Pt microelectrodes (Fig. 2). The left electrode in the nucleation core was designated as the WE. Different CEs were used having areas that spanned five orders of magnitude and included the identical right electrode in the core (XS), larger microfabricated electrode in the adjacent channel (S), and two Pt wire macro electrodes placed exterior to the channel but in contact with the electrolyte (L and XL, Fig. 3). Although CE-WE distances vary across these cases, the associated iR drop is negligible compared to the interfacial potential.

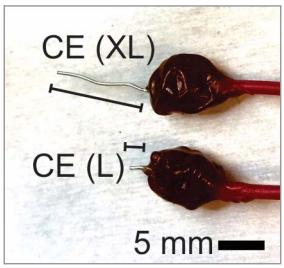

Size	GSA (μm^2)
XS	2.25×10^2
S	2.50×10^3
L	1.75×10^6
XL	1.59×10^7

Figure 3: (Left) Two macroscale Pt wire CEs. The wire diameters were 0.5 mm. (Right) Table showing the geometric surface areas (GSA) of the tested CEs.

Room temperature 1 × phosphate buffered saline (PBS) served as the electrolyte and filled the microchannel via fluid ports (Fig. 2 & 4). Devices were mounted in a custom acrylic test fixture which allowed them to be immersed in PBS (Fig. 5). A potentiostat obtained electrochemical impedance spectroscopy (EIS) measurements. A sourcemeter and oscilloscope were configured as shown in Fig. 6 to control the electrochemical cell with an Ag|AgCl reference electrode (RE). For voltage cycling experiments, WE-CE voltage was cycled at ±100 mV/s; user input switched the ramp's polarity upon observation of H_2/O_2 evolution (3 trials/device/CE size). For pulsing experiments, H_2 nanobubbles were generated ($2H^+ + 2e^- \rightarrow H_2$) under current control (-0.6 µA, 6 s; 8 trials/device/CE size on 3 devices). MATLAB scripts extracted nanobubble volume from microscope images acquired at 10 fps (Fig. 9).

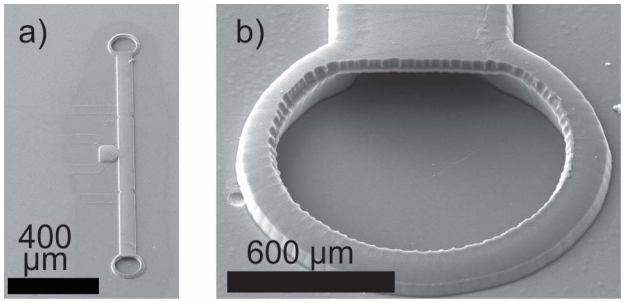

Figure 4: a) SEM image of fabricated device. b) Close up detail of the bottom fluid port, showing the opening to the microchannel.

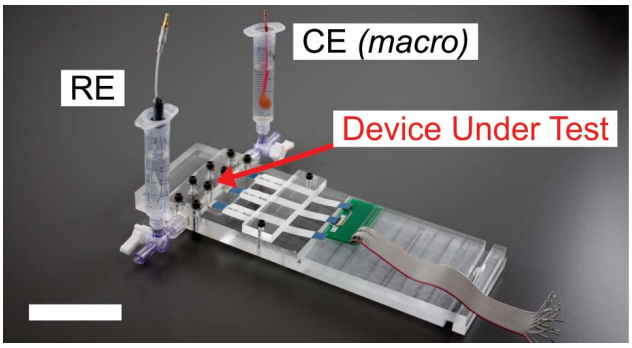

Figure 5: Testing setup for optical and electrochemical data acquisition. The RE was Ag|AgCl (3M NaCl). Scale bar = 5 cm.

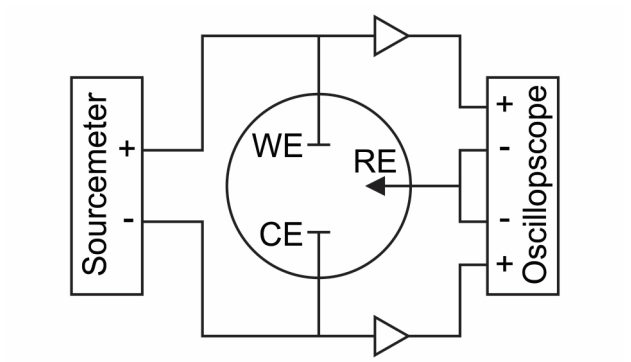

Figure 6: Circuit diagram of the device testing setup. A sourcemeter applied and measured voltage or current between the WE and CE. A 2-channel oscilloscope with unity gain voltage buffers measured voltage of the WE and CE with respect to RE.

RESULTS AND DISCUSSION

Electrochemical Impedance Spectroscopy

EIS prior to bubble generation revealed low inter-device variability. WEs displayed similar electrochemical impedance magnitude and phase (Fig. 7). This ensures that all tested devices were comparable.

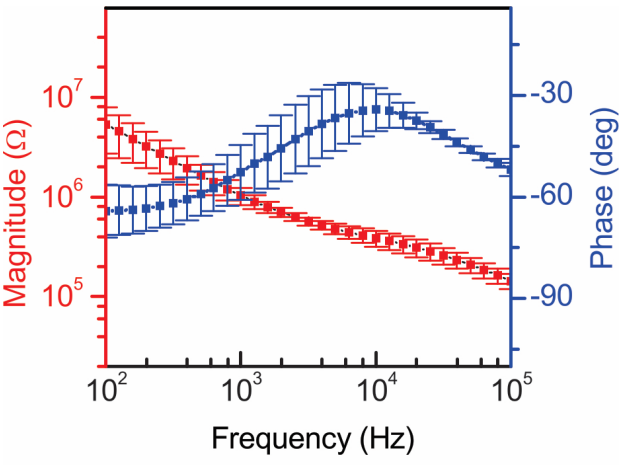

Figure 7. The EIS reveals that the WEs across the 4 tested devices have similar electrochemical impedance magnitude and phase.

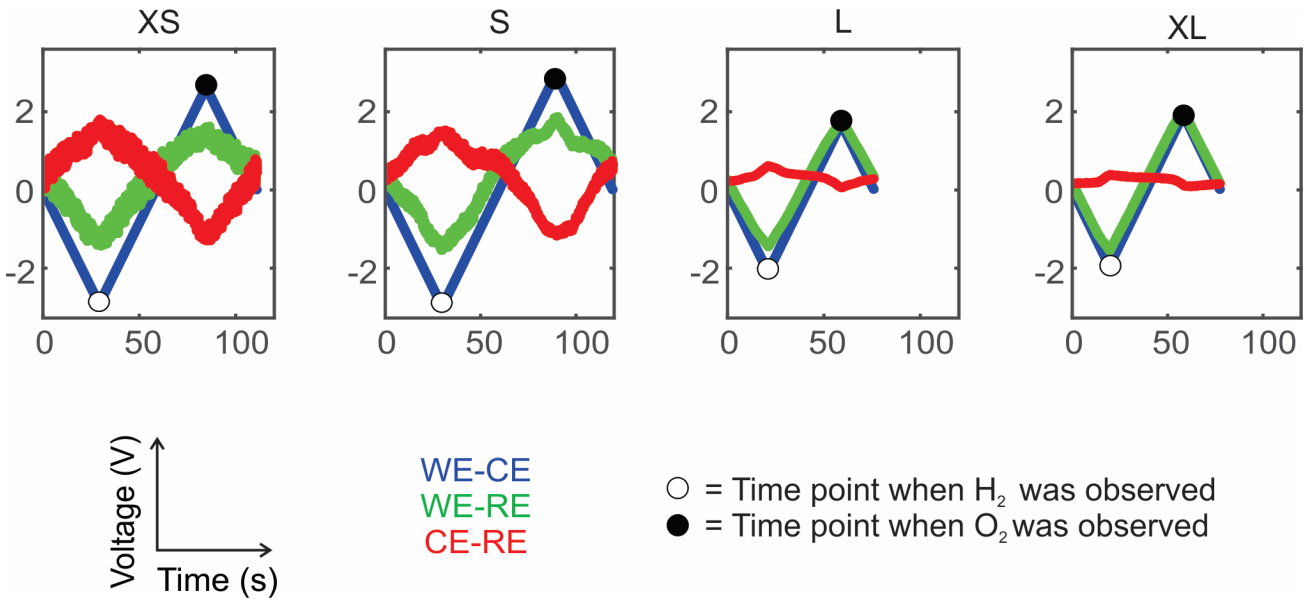

Figure 8: Representative voltage vs. time plots. Applied voltage was ramped at -100 mV/s until H_2 evolution was observed in real time. At that instant, voltage was ramped at +100 mV/s until O_2 evolution was observed and then ramped at -100 mV/s to 0 V. For larger CE sizes, power consumption is reduced because less applied voltage is required to generate gas when the voltage drop occurs mainly at the WE-electrolyte interface.

Voltage Cycling

For voltage cycling experiments (Fig. 8), the hydrogen evolution reaction (HER) and oxygen evolution reaction (OER) were consistently observed across all trials. The total applied voltage (blue) and the WE-RE voltage (green) were more closely matched when a larger CE were used, confirming that electrode polarization was successfully localized at the WE-electrolyte interface. The timepoints at which HER or OER reactions occurred revealed that lower total applied voltage magnitude was required to generate gas for larger counter electrodes. (Fig. 8). Larger CE size experiments also exhibited less noise.

Pulse Tests: Bubble Energy

For pulsing experiments, the average total applied voltage between the WE-CE pair, average current during the pulse, and pulse duration were multiplied to compute the energy required to generate a single nanobubble. Table 1 reveals that larger CEs have the capability to reduce energy consumed per bubble generated.

This energy reduction benefit was obtained between sizes S and L (2.5×10^4 to 1.75×10^6 μm^2), illustrating that larger CEs are more energy efficient. Up to 44% in energy savings was achieved when comparing between XS and L (1.99 and 1.12 µJ) CEs.

Pulse Tests: Bubble Volume

Bubble growth and dissolution dynamics were successfully tracked by using high frame rate image acquisition software and custom MATLAB algorithms (Fig. 9 and 10).

Size	WE-CE Voltage During Pulse (V)	Energy Per Bubble (µJ)
XS	-3.31 ± 0.26	-1.99 ± 0.16
S	-3.16 ± 0.13	-1.90 ± 0.08
L	-1.87 ± 0.03	-1.12 ± 0.02
XL	-1.98 ± 0.10	-1.19 ± 0.06
N = 24 Per Size Condition; Mean ± S.D.		

Table 1: During the current pulse, the applied voltage was measured. The energy per bubble was tabulated by multiplying the average total applied voltage throughout the pulse by the constant -0.6 µA current applied for 6 s.

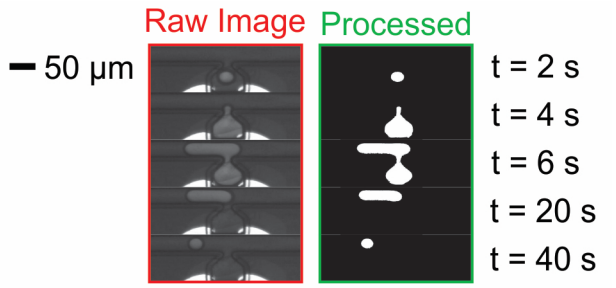

Figure 9: Representative sequential frames showing bubble volume experiments. Custom MATLAB algorithms were used to process raw images into binary images in order to quantify bubble area.

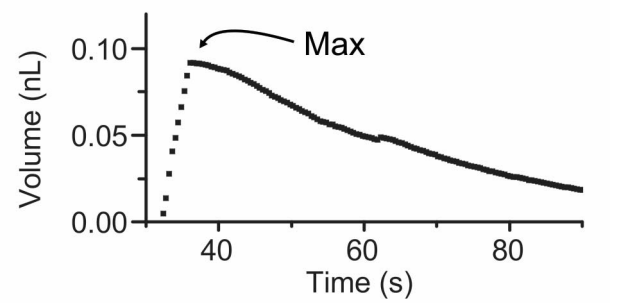

Figure 10: A representative time course of H_2 bubble volume for a single current pulse. An approximation of the total bubble volume can be obtained by multiplying the bubble area as determined via the MATLAB algorithm by channel height (as measured by a profilometer). The maximum can then be easily extracted.

The average maximum bubble volumes were 0.09, 0.12, 0.11, and 0.08 nL for the various CE sizes (XS, S, L, and XL; respectively). Associated standard error (SE) averaged between datasets with appropriate statistical methods revealed that larger CEs yielded smaller SE in bubble volume. The best SE in one XL dataset consisting of 8 trials was 1.1 pL which corresponds to approximately 5 × improvement over the 5.1 pL average SE in the XS case (Fig. 10). These results suggest the advantage of increased bubble volume precision when employing larger CEs for microscale electrochemical devices. Although Pt wires were used here, equivalent area thin-film electrodes should result in a similar benefit.

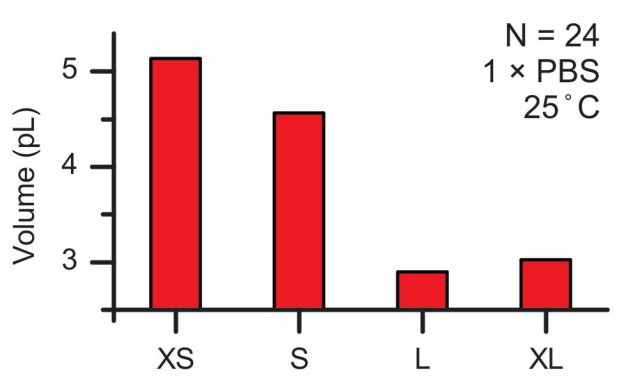

Figure 11: From maximum bubble volume data, the standard error was computed and plotted by CE size. Larger CE provided greater precision in nanobubble control than the smaller micro CEs.

CONCLUSION

This work examined the effect of CE size on the performance of electrolytic nanobubble generators used in microfluidic devices. Basic electrochemical principles suggest the use of a large surface area counter electrode to improve control and efficiency. A systematic study was conducted and supported increase of CE size. Specifically, larger area CEs resulted in decreased power consumption per generated nanobubble and improved precision of bubble volume control.

ACKNOWLEDGEMENTS

This work was supported in part by the National Science Foundation under award numbers ECCS-1231994, IIP-1601340, and IIP-1827773 and the Viterbi Mousetrap Fund. The authors would like to thank Drs. Dan Merrill and Alex Baldwin for the fruitful discussions which helped frame this work. In additional, many thanks go out to members of the USC Biomedical Microsystems Laboratory for their assistance.

REFERENCES

[1] L. Hsu, J. Ramunas, J. Gonzalez, J. G. Santiago, and D. G. Strickland, "Toward an electrolytic micropump actuator design with controlled cyclic bubble growth and recombination," *ECS Trans.*, vol. 35, no. 30, pp. 3–11, 2011.

[2] S. Lee, E. Loth, and C. Liu, "Micro-bubbles generated on electrolytic arrays and matrices and released in a water channel," *Exp. Fluids*, vol. 38, no. 5, pp. 672–682, 2005.

[3] S. Z. Hua, F. Sachs, D. X. Yang, and H. D. Chopra, "Microfluidic Actuation Using Electrochemically Generated Bubbles," *Anal. Chem.*, vol. 74, no. 24, pp. 6392–6396, 2002.

[4] A. Bouakaz, P. J. A. Frinking, N. De Jong, and N. Bom, "Noninvasive measurement of the hydrostatic pressure in a fluid-filled cavity based on the disappearance time of micrometer-sized free gas bubbles," *Ultrasound Med. Biol.*, vol. 25, no. 9, pp. 1407–1415, 1999.

[5] L. Yu, C. A. Gutierrez, and E. Meng, "An Electrochemical Microbubble-Based MEMS Pressure Sensor," *J. Microelectromechanical Syst.*, vol. 25, no. 1, pp. 144–152, 2016.

[6] A. Bard and L. Faulker, *Electrochemical Methods: Fundamentals and Applications, 2nd Edition*. John Wiley & Sons, Inc., 2000.

CONTACT

*E. Yoon; tel: +1-213-821-3897; eugenejy@usc.edu
*E. Meng; tel: +1-213-821-3949; ellismeng@usc.edu